U.S. CLIVAR

Spring 2013, Vol. 11, No. 1

VARIATIONS

Decadal variability and predictability

Mike Patterson, Director

An ambitious set of coordinated modeling experiments has been undertaken as part of the fifth phase of the Coupled Model Intercomparison Project (CMIP5). The experiments are investigating whether the climate models used for climate change projections can capture not only the impact of the changing atmospheric composition, but also the evolution of slow natural variations of the climate system when initialized with ocean observation data. A decadal-scale predictive capacity, if determined to be feasible, would help fill the temporal gap between seasonal-to-interannual climate prediction and centennial-scale climate change projections, and address the growing user demand for decadal-scale climate information.

In anticipation of the decadal modeling experiments, U.S. CLIVAR initiated a Decadal Predictability Working Group (DPWG) in January 2009 to understand sources of predictability for climate variations on decadal timescales, and to provide a common framework for assessing decadal predictions. A summary of the DPWG objectives, activities and products is provided in the first article here.

Complimenting the work of the DPWG, U.S. CLIVAR agencies solicited proposals for Coupled Model Experiment Project (CMEP

Overview of U.S. CLIVAR Working Group on Decadal Predictability

Lisa Goddard
Columbia University/International Research Institute for Climate and Society

In 2009, U.S. CLIVAR initiated a limited lifetime Working Group on Decadal Predictability (DPWG) in recognition of the importance of decadal variability and its societal impacts and in recognition of the growing activity within the scientific community. At that time several international and national efforts were underway to produce experimental decadal predictions based on dynamical climate models, such as the initialized decadal predictions and hindcasts that are part of the IPCC Fifth Assessment Report. These decadal predictions potentially complement projections of expected changes in climate that are based primarily on forcing from increasing greenhouse gasses. Given that even climate change adaptation efforts typically target only a 10-20 year horizon for implementation and evaluation (rather than the end of the 21st Century), demand has been increasing for decadal climate information. At these timescales, natural decadal-scale variability can be more important than anthropogenic trends.

The DPWG sought to advance the assessment of decadal predictability. It had two main objectives. The first was to provide an overview of and findings from methodologies to separate decadal variations and anthropogenically forced trends. One could argue that this distinction is immaterial, since we experience the two together. However, an understanding of the relative importance of anthropogenic change and natural variability to regional climate is useful for attribution of recent climate, to set appropriate expectations of future climate changes, and to test the ability of models to correctly simulate recent climate for the right reasons. We found that there is no method to cleanly separate variability from change, though some methods may indicate changes in the characteristics of climate variability in the models (Solomon et al. 2011).

IN THIS ISSUE

2011) to enable diagnostic analysis of late 19th - 20th century simulations and analysis of the CMIP5 initialized decadal hindcasts and predictions. Twenty-seven small grants were awarded by four agencies (NSF, NOAA, NASA and ONR) supporting analyses of oceanic and atmospheric modes of variability, regional climate and monsoon variability and trends, hydrological cycle behavior, extreme events, carbon cycle feedbacks, and aerosol effects (www.usclivar.org/resources/cmep2011_awards). Results from six CMEP 2011 decadal variability and predictability studies are presented in this issue.

New Science Plan

The U.S. CLIVAR Scientific Steering Group is leading the drafting of a new Science Plan for the next 15-year era of the program with input from members of its panels and scientists in the community. A draft of the Plan will be available for public review from June 12 - July 3, 2013. We welcome your input to improve the plan. Please watch for the notification to be sent to subscribers of the newsletter announcing the opening of the public review via an online system on the U.S. CLIVAR website.

U.S. CLIVAR VARIATIONS

Editors: Mike Patterson, Director
Jennifer Mays, Program Specialist
U.S. CLIVAR Project Office
1717 Pennsylvania Ave NW, Ste 850
Washington, DC 20006
202.419.1801 www.usclivar.org

The second objective of the DPWG was to develop a framework to quantify the ability of state-of-the-art climate models to predict decadal variability. Since the climate over the coming decade is a result of both natural and anthropogenic factors, the decadal predictions can potentially provide the necessary initial conditions to predict the former as well as a more realistic starting point to reduce model biases in the latter. The framework we developed focuses mainly metrics connected to relative accuracy: Is the predicted information more accurate than assuming climatological averages? Are the decadal predictions a more accurate representation of the observations than the climate change projections? Our accuracy metric – the mean squared skill score – is related to both correlation and to conditional bias, or response bias. As with prediction studies for seasonal-to-interannual variability, we found that the specific results varied among models, but that overall temperature is better predicted than precipitation. We also found that there is currently very little additional prediction skill over land provided by the initialized predictions (Goddard et al. 2012; http://clivar-dpwg.iri.columbia.edu). However, we concluded, as have others, that the IPCC experimental design of the decadal predictions, with initial conditions only every 5 years (yielding only 10 hindcasts) and small ensemble size, hinders the ability to estimate model skill. On a positive note, more information can likely be mined through appropriate bias corrections and multi-model ensembles.

The study of decadal variability and its prediction continues to draw together an increasing collection of scientists. For climate science, this is a frontier. We currently have very little understanding of what can be predicted with any accuracy between the interannual timescale of El Nino and the multi-decade timescale of anthropogenic climate change. Important challenges still remain in our observational description of decadal-scale variability, in designing the observational networks needed to capture the relevant processes and initialize models, in model simulations of that variability, and our understanding of what processes can and must be predicted in order to provide the comingled evolution of variability and change. Important next steps being undertaken in the study of decadal prediction are investigations of the dynamics of specific events in observations and models, such as the mid-1970s shift in the Pacific and the mid-1990s shift in the North Atlantic. These types of studies will hopefully shed more light on the outstanding scientific challenges we face. The importance of this area of study cannot be underestimated. This is scientific information that can inform development, planning, and policy. As such, work on decadal climate should be viewed as an opportunity to provide sound guidance on our current understanding of potential value, as well as critical gaps, of this information.

References

Goddard, L., A. Kumar, A. Solomon, D. Smith, G. Boer, P. Gonzalez, V. Kharin, W. Merryfield, C. Deser, and S. J. Mason, et al., 2013: A verification framework for interannnual-to-decadal prediction experiments. *Climate Dyn.*, **40**, 245-272, doi:10.1007/s00382-012-1481-2.

Solomon, A., L. Goddard, A. Kumar, J. Carton, C. Deser, I. Fukumori, A. Greene, G. Hegerl, B. Kirtman, Y. Kushnir, M. Newman, D. Smith, D. Vimont, T. Delworth, J. Meehl, and T. Stockdale, 2010: Distinguishing the roles of natural and anthropogenically forced decadal climate variability: Implications for prediction. *Bull. Amer. Meteor. Soc.,* **42**, 141-156, doi:10.1175/2010BAMS2962.1.

Using initialized decadal hindcasts to assess simulated 50-year trends in the tropical Indo-Pacific Ocean

Amy Solomon
PSD/ESRL/NOAA and CIRES/University of Colorado

Introduction: The Climate Model Intercomparison Project phases 3 and 5 (CMIP3 and CMIP5) organized an assessment of climate model simulations forced with an estimate of 20th-21st century external forcings (greenhouse gases, volcanic emissions, solar cycle variability, and aerosols) in order to verify and validate climate models used for projections of future climate change. Studies of CMIP3 ensembles clearly demonstrate that model uncertainty is the dominant source of uncertainty for projections of globally averaged surface temperature on decadal time scales (see Hawkins and Sutton 2009, 2011). Further, these studies show that for regional averages uncertainty due to model uncertainty is of the same order as internal variability.

This study focuses on the region of the tropical Indo-Pacific Ocean, where sea surface temperatures (SST) in the Warm Pool region (18°N-18°S, 60°-165°E) have warmed by approximately 0.5°C since 1961 (Figure 1). Climate change has been attributed to teleconnections forced from the tropical Indo-Pacific both regionally, for example the persistent drought of 1998-2002 over the U.S. (Hoerling and Kumar 2003), and worldwide (Diaz and Markgraf 1992; Glantz 2001; Alexander et al. 2002). This highlights the need to identify model biases that may be limiting the accuracy of climate change projections in this region. Specifically, it is necessary to assess SST trend patterns since differing dominant feedbacks result in different Indo-Pacific SST trend patterns (e.g., Clement et al. 1996; Seager and Murtugudde 1997; Held and Soden 2006), which has significant implications for global climate change (e.g., Schneider et al. 1997; Shin and Sardeshmukh 2010).

The World Climate Research Program's (WCRP) Working Group on Coupled Modeling has carried out a coordinated set of model experiments for the Intergovernmental Panel on Climate Change Fifth Assessment (AR5) that includes, for the first time, simulations of decadal climate prediction (hereafter referred to as initialized decadal hindcasts, see WCRP Joint Scientific Committee Session 29 Report). CMIP5 initialized decadal hindcasts provide an opportunity

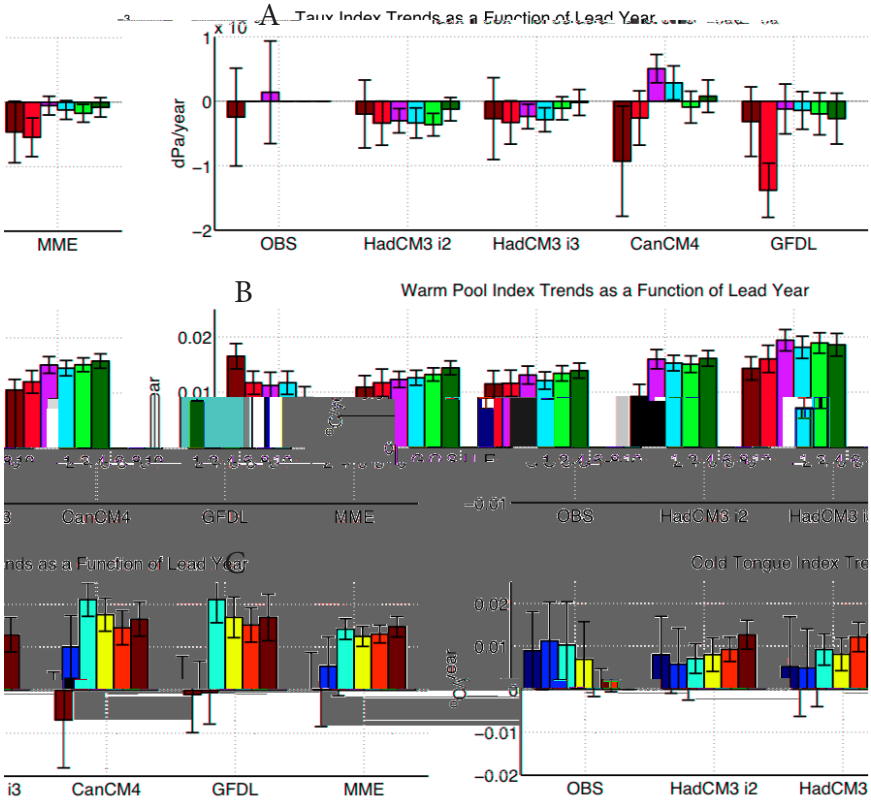

Figure 1. A) Taux index 50-year linear trends as a function of lead year, in units of dPa/year. B) Warm Pool index 50-year linear trends as a function of lead year, in units of °C/year. C) Cold Tongue index 50-year linear trends as a function of lead year, in units of °C/year. Trends for lead years 1,2,4,6,8,10 shown for ensemble mean hindcasts, as indicated in (B). Trends calculated from start dates between 1960-2010. MME indicates multi-model ensemble mean. Observed 1961-2010 trends estimated using three data assimilations (marked, "G", "O", "S") and a best estimate from 4 SST reconstructions with (marked "A") and without (marked "R") ENSO variability. Error bars show 95% confidence intervals. Models, verification datasets, and techniques described in the appendix.

to assess "model response uncertainties" by identifying how modeled trends diverge from an observed ocean state estimate in the initialized decadal hindcasts to the uninitialized trend pattern over a 10-year forecast.

Results: In this article we present results of trends in SSTs and zonal wind stress from a larger study on systematic biases in the Indo-Pacific Ocean. We use two indices to describe, to first order, the equatorial SST trend pattern in the Indo-Pacific Ocean; the Warm Pool index (previously defined) and the Cold Tongue index (SSTs averaged over 5°N-5°S, 170°E-70°W). A third index is used to describe the equatorial wind stress trends, the Pacific zonal mean zonal wind stress index (zonal wind stress averaged over 5°N-5°S, 120°E-70°W; referred to as the taux index). These three indices are used to describe trends in the Walker circulation, the asymmetric circulation in the tropical Indo-Pacific where convection in the Warm Pool region forces upward motion that subsides in the central-eastern Pacific. There is currently an active debate as to whether the Walker circulation will weaken or strengthen as a response to an increase in greenhouse gases (see discussion in DiNezio et al. 2013). However, this response may be a function of time scale, where the equatorial Indo-Pacific SST gradient may strengthen on fast time scales (e-folding time scale of approximately 5 years) but weaken on slow time scales (Held et al. 2010). Held et al (2010) posit that the slow response has not yet emerged during the historical period based on a range of model experiments.

Forecasted trends are calculated as follows: trends at lead year 1 are calculated from the time series of the first year of the 50 start dates, trends at lead year 2 are calculated from the time series of the second year of the 50 start dates, etc. In tropical Pacific SSTs, the externally forced signal emerges from the signal due to initial conditions after approximately 4 years and all information from the initialization is lost in approximately 6 years (Branstator and Teng 2010). We therefore use forecasted trends for lead years 6-10 as estimates of uninitialized trends. Decadal hindcasts and verification datasets used in this study are described in the appendix.

Ensemble mean 50-year Warm Pool, Cold Tongue and taux trends as a function of lead year are presented in Figure 1. Looking at the observed trends first (leftmost column), there is a systematic warming trend in all of the observed Warm Pool index time series even though these trends differ by up to a factor of 2. This is not the case for the taux and Cold Tongue trends, where large variability obscures identifying whether these trends have increased or decreased over the 1961-2010 period. There is a tendency for a warming trend in the Cold Tongue index, however only one of these time series is significant beyond the 95% level. Since large uncertainty in the Cold Tongue index is primarily due to ENSO variability we also show an estimate of an ENSO residual trend (marked "R" in Figure 1, where ENSO variability has been removed following the technique of Solomon and Newman (2012)). Removing ENSO variability reduces the Cold Tongue warming trend by over 68%, which is useful in assessing the magnitude of the ensemble mean simulated trends at long leads but uncertainty in the ENSO residual index is too large to validate the sign of the simulated trends.

To identify the impact of the initialization method on the long-lead trends we use two ensembles of HadCM3 initialized hindcasts, one that employed anomaly initialization (HadCM3 i2) and one that employed full-field initialization (HadCM3 i3). Even though full-field initialized hindcasts have large model drift from the observed climatology to the model climatology (see Kim et al. 2012), the bias-corrected trends shown in Figure 1 are relatively insensitive to the initialization method.

Looking at the multi-model ensemble mean (MME) trends in Figure 1, a significant warming trend is seen in both the Warm Pool and Cold Tongue trends by lead year 4. This is not the case for the MME taux trends, where even though confidence intervals narrow for increasing lead years, trends for lead years 4-10 are not significantly different from zero. There is an indication that the Warm Pool trends may be just outside the observed estimates based on all verification datasets except ECDA. Cold Tongue trends for lead years 4-10 are 5 times larger than the ENSO residual estimate.

The loss of information in the initial conditions in all three MME indices is seen in the narrowing of the confidence intervals from lead year 1 to lead year 4, where after confidence intervals are approximately constant. It

is between leads years 1 and 4 that the divergence from the initial observed ocean state estimate can be seen, for example in the discontinuous jump in all MME trends between leads years 2 and 4. In our complete study we extend this analysis to subsurface fields in order to investigate the processes that cause Warm Pool and Cold Tongue warming trends for increasing lead years that exceed estimates from data assimilations and SST reconstructions.

Appendix: Methods, Models and Data: We apply our analysis to four sets of initialized decadal hindcasts archived in the CMIP5 database (Taylor et al. 2012) that are initialized yearly from 1960-2009. Each start date has 10 ensemble members with perturbed initial conditions. These hindcasts take into account changes in external forcings such as greenhouse gases, solar activity, stratospheric aerosols associated with volcanic eruptions and anthropogenic aerosols. The first two ensembles use the UK Met Office coupled climate model HadCM3 configured with a horizontal resolution of 2.5°x2.5° in the atmosphere and 1.25° in the ocean (Gordon et al. 2000). The HadCM3-i2 ensemble is anomaly initialized (observed anomalies and the model's mean climate are used as initial conditions) and the HadCM3-i3 ensemble is initialized with full fields (observed anomalies and climate mean states are used as initial conditions). The third ensemble uses the Canadian Centre for Climate Modelling and Analysis CanCM4 (Arora et al. 2011; Merryfield et al. 2013), and is full field initialized. The fourth ensemble uses the NOAA Geophysical Fluid Dynamics Laboratory CM2.1 (Delworth et al. 2006; Chang et al. 2013) and is anomaly initialized. A multi-model ensemble mean (MME) is formed by averaging time series from the 4 ensembles. All fields are interpolated to the HadCM3 2.5°x2.5° grid. Only results using annual and ensemble means are presented in this article.

Annual mean anomalies are bias corrected as a function of lead-time, where the model forecast anomaly is calculated as $Y'_{j\tau} = Y_{j\tau} - \bar{Y}_{\tau}$ where $\bar{Y}_{\tau}$ is the ensemble-average forecast as a function of lead-time τ, $Y'_{j\tau}$ is the anomaly of the raw forecast with respect to the ensemble average, j is the starting year. $\bar{Y}_{\tau}$ is calculated as $\frac{1}{n}\sum_{j=1}^{n} Y_{j\tau}$.

Linear trends are calculated using the method of least squares linear regression. Confidence intervals are estimated using a Student's t distribution (Bendat and Piersol, 2000). Trends are estimated to be significantly different from a zero trend when they exceed the 95% level.

Three data assimilations and four SST reconstructions are used to verify the hindcasts. The data assimilations are the European Centre for Medium-range Weather Forecasts (ECMWF) Ocean Reanalysis System 4 (ORAS4, Balmaseda et al. 2013), the Geophysical Fluid Dynamics Laboratory Ensemble Coupled Data Assimilation V3.1 (ECDA, Chang et al. 2013), and the Simple Ocean Data Assimilation version 2.1.6 (SODA, Carton and Giese 2008). The SST reconstructions are the Hadley Centre Sea Ice and SST dataset version 1.1 (HadISST, Rayner et al. 2003), the National Oceanic and Atmospheric Administration Extended Reconstruction SST version 3b dataset (ERSST, Smith et al. 2008), Lamont Doherty Earth Observatory SST version 2 (KAPLAN, Kaplan et al. 1998), Centennial in Situ Observation Based Estimates of SST (COBE, Ishii et al. 2005). The four reconstructions are averaged to form a "best estimate", marked with an "A" in Figure 1. Also shown in Figure 1 is the best estimate of the SST trends where ENSO variability has been removed following the technique developed in Solomon and Newman (2012), marked with "R".

Acknowledgments:

The author thanks Matt Newman for helpful comments. We acknowledge the World Climate Research Programme's Working Group on Coupled Modelling, which is responsible for CMIP, and we thank the climate modeling groups (listed in this paper) for producing and making available their model output. For CMIP the U.S. Department of Energy's Program for Climate Model Diagnosis and Intercomparison provides coordinating support and leads development of software infrastructure in partnership with the Global Organization for Earth System Science Portals. This work has been supported by grants from the NOAA OAR CVP program and NSF AGS 1125561.

References

Alexander, M. A., I. Blade, M. Newman, J. R. Lanzante, N.-C. Lau, and J. D. Scott, 2002: The Atmospheric Bridge: The influence of ENSO teleconnections on air-sea interaction over the global oceans. *J. Climate*, **15**, 2205-2231.

Arora, V., and Coauthors, 2011: Carbon emission limits required to satisfy future representative concentration pathways of greenhouse gases. *Geophys. Res. Lett.*, **38**, L05805, doi:10.1029/2010GL046270.

Balmaseda, M. A., K. Morgensen, and A. Weaver, 2013: Evaluation of the ECMWF Ocean Reanalysis ORAS4. *Q. J. Roy. Met.*, doi:10.1002/qj.2063.

Bendat, J. S., and A. G. Piersol, 2000: Random data analysis and measurement procedures. ISBN 0471317330, P113.

Branstator, G., and H. Teng, 2010: Two Limits of Initial-Value Decadal Predictability in a CGCM. *J. Climate*, **23**, 6292–6311. doi:10.1175/2010JCLI3678.1.

Carton, J. A., and B. S. Giese, 2008: A reanalysis of ocean climate using Simple Ocean Data Assimilation (SODA). *Mon. Wea. Rev.*, **136**, 2999-3017.

Chang, Y.-S., S. Zhang, A. Rosati, T. Delworth, and W. F. Stern, 2013: An assessment of oceanic variability for 1960-2010 from the GFDL ensemble coupled data assimilation, *Climate Dyn.*, **40**, 775-803, doi:10.1007/s00382-012-1412-2.

Clement, A. C., R. Seager, M. A. Cane, and S. E. Zebiak, 1996: An ocean dynamical thermostat. *J. Climate,* **9**, 2190–2196.

Delworth, T. L., and Coauthors, 2006: GFDL's CM2 global coupled climate models. part I: Formulation and simulation characteristics. *J. Climate*, **19**, 643–674.

Diaz, H. F., and V. Markgraf, 1992: El Niño: Historical and paleoclimatic aspects of the Southern Oscillation. Cambridge University Press, Cambridge, 476 pp.

DiNezio, P. N., G. A. Vecchi, and A. C. Clement, 2013: Detectability of Changes in the Walker Circulation in Response to Global Warming. *J. Climate*, doi:10.1175/JCLI-D-12-00531.1

Glantz, M. H., 2001: Currents of Change: Impacts of El Nino and La Nina on climate and society. Cambridge University Press, Cambridge, 252 pp.

Gordon, C., C. Cooper, C. A. Senior, H. Banks, J. M. Gregory, T. C. Johns, J. F. B. Mitchell, and R. A. Wood, 2000: The simulation of SST, sea ice extents and ocean heat transport in a version of the Hadley Centre coupled model without flux adjustments. *Clim. Dyn.*, **16**, 147–168.

Hawkins, E., and R. T. Sutton, 2009: The potential to narrow uncertainty in regional climate predictions. *Bull. Am. Meteorol. Soc.*, **90**, 1095-1107. ISSN 1520-0477 doi:10.1175/2009BAMS2607.1.

Hawkins, E., and R. T. Sutton, 2011: The potential to narrow uncertainty in projections of regional precipitation change. *Clim. Dyn.,* **37**, 407-418. ISSN 1432-0894 doi: 10.1007/s00382-010-0810-6.

Held, I. M., and B. J. Soden, 2006: Robust responses of the hydrological cycle to global warming. *J. Climate*, *19*, 5686-5699, doi:10.1175/JCLI3990.1.

Held, I. M, M. Winton, K. Takahashi, T. Delworth, F. Zeng, and G. K. Vallis, 2010: Probing the fast and slow components of global warming by returning abruptly to preindustrial forcing. *J. Climate*, **23**, 2418-2427, doi:10.1175/2009JCLI3466.1.

Hoerling, M., and A. Kumar, 2003: The Perfect Ocean for Drought. *Science*, **299**, 691-694.

Ishii, M., A., Shouji, S. Sugimoto, and T. Matsumoto, 2005: Objective analyses of SST and marine meteorological variables for the 20th century using ICOADS and the Kobe Collection. Int. *J. Climatol.*, **25**, 865–879.

Kaplan, A., and Coauthors, 1998: Analyses of global sea surface temperature 1856–1991. *J. Geophys. Res.*, **103**, 18,567–18,589, doi:10.1029/97JC01736.

Kim, H. M., P. J. Webster, and J. A. Curry, 2012: Evaluation of short-term climate change prediction in multi-model CMIP5 decadal hindcasts. *Geophys. Res. Lett.*, **39**, L10701, doi:10.1029/2012GL051644.

Merryfield, W. J., W. Lee, G. J. Boer, V. V. Kharin, J. F. Scinocca, G. F. Flato, R. S. Ajayamohan, Y. Tang, and S. Polavarapu, 2013: The Canadian Seasonal to Interannual 1 Prediction System. Part I: Models and initialization. *Mon. Wea. Rev.*, doi:10.1175/MWR-D-12-00216.1.

Rayner, N. A., and Coauthors, 2003: Global analyses of sea surface temperature, sea ice, and night marine air temperature since the late nineteenth century. *J. Geophys. Res.*, **108**, 4407, doi:10.1029/2002JD002670.

Schneider, E. K., R. S. Lindzen, and B. P. Kirtman, 1997: A tropical influence on global climate. *J. Atmos. Sci.*, **54**, 1349-1358.

Seager, R., and R. Murtugudde, 1997: Ocean dynamics, thermocline adjustment, and regulation of tropical SST. *J. Climate,* **10**, 521–534.

Shin S.-I., and P. D. Sardeshmukh, 2010: Critical influence of the pattern of Tropical Ocean warming on remote climate trends. *Clim. Dyn.*, **36,** 1577-1591.

Smith, T. M., R. W. Reynolds, T. C. Peterson, and J. Lawrimore, 2008: Improvements to NOAA's historical merged land-ocean surface temperature analysis (1880-2006). *J. Climate,* **21**, 2283-2296.

Solomon, A., and M. Newman, 2012: Reconciling disparate 20th century Indo-Pacific ocean temperature trends in the instrumental record. *Nature Climate Change*, **2**, 691-699, doi:10.1038/NCLIMATE1591.

Taylor, K. E., R. J. Stouffer, and G. A. Meehl, 2012: An Overview of CMIP5 and the Experiment Design. *Bull. Amer. Meteor. Soc.*, **93**, 485–498. doi:10.1175/BAMS-D-11-00094.1.

Join us in Baltimore, MD for the second joint meeting of the UK RAPID & US AMOC science programs. To encourage integration of observations and theory, and merger of results across geographic areas, the meeting will address three themes:

- **Observations and dynamics of seasonal-to-interannual timescales**
- **Observations and dynamics of decadal to multi-centennial timescales**
- **Climate impacts**

Registration and agenda online now at: **www.usclivar.org/meetings/amoc2013**

Evaluation of short-term climate change prediction in multi-model CMIP5 decadal hindcasts

Hye-Mi Kim[1], Peter J. Webster[2], and Judith A. Curry[2]
[1]School of Marine and Atmospheric Sciences, Stony Brook University, New York
[2]School of Earth and Atmospheric Science Georgia Institute of Technology, Georgia

The prediction of decadal climate variability against a background of global warming is one of the most important and challenging tasks in climate science. Not only does natural variability have a large-amplitude influence over broad regions of the globe, it is an integral component of climate variability that modulates low-frequency climate phenomena as well as extreme climate events such as tropical cyclone activity. The Coupled Model Intercomparison Project Phase 5 (CMIP5) has devised an innovative experimental design to assess the predictability and prediction skill on decadal time scales of state-of-the-art climate models, in support of the Intergovernmental Panel on Climate Change (IPCC) 5th Assessment Report (Taylor et al. 2012). We compare the ability of currently available CMIP5 decadal hindcasts to simulate the mean climate and decadal climate variability from individual coupled models and a multi-model ensemble (MME). We focus on the surface temperature and two dominant internal climate modes, the Atlantic Multidecadal Oscillation (AMO) and Pacific Decadal Oscillation (PDO).

CMIP5 decadal hindcast/forecast simulations of seven state-of-the-art ocean-atmosphere coupled models are assessed. Each decadal prediction consists of simulations over a 10 year period each of which are initialized every five years from climate states of 1960/1961 to 2005/2006. The equally weighted average from total 52 ensemble members of seven hindcast experiments provides the values for the MME. A brief summary of each model's experimental configuration is presented in Kim et al. (2012). The model prediction skill is examined by comparing the annual mean surface temperature from the observation and hindcasts of each model. Most of the models overestimate trends, whereby the models predict less warming or even cooling in the earlier decades compared to observations and too much warming in recent decades (Figure 1).

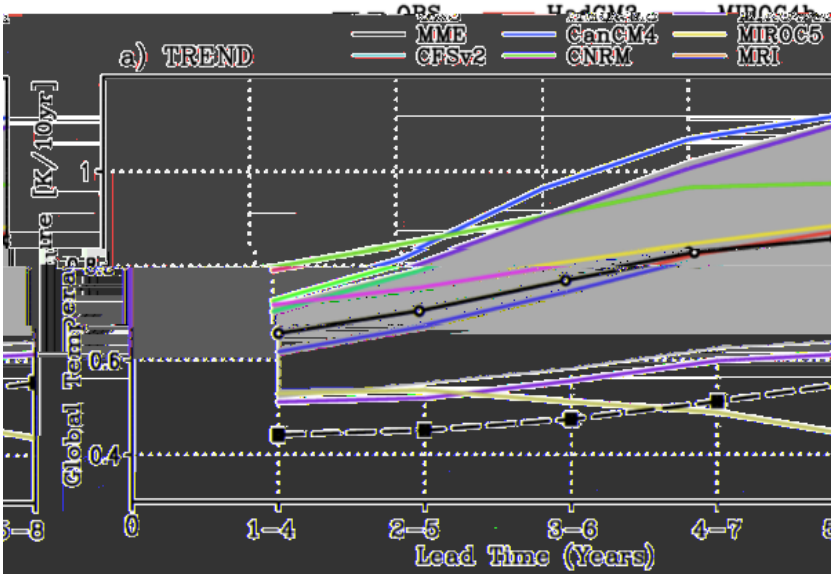

Figure 1. Trend [K/10yr] for the global mean annual temperature anomaly predicted by MME and ensemble-mean of each CMIP5 decadal hindcasts as a function of lead time. Black dashed line represents the trend in the observation. Gray shades represent the ranges of one standard deviation of the ensemble-mean in each hindcasts.

All models show high prediction skill for surface temperature over the Indian, North Atlantic and western Pacific Oceans up to 6-9 years where the externally forced component and low-frequency climate variability is dominant. Comparing the globally averaged skill for each model's hindcasts shows the highest skill occurring for the MME over the entire period. The AMO index is predicted in most of the models with significant skill, while the PDO index shows relatively low predictive skill (Figure 2). The multi-model ensemble has in general better-forecast quality than the single-model systems for global mean surface temperature, AMO and PDO.

Although the MME does not outperform all of the constituent models for every forecast skill metric, it has in general better forecast quality than the single models for global mean temperature, AMO and PDO. This study partly supports the utility of the multi-model ensemble approach in overcoming the systematic model biases from individual models and in enhancing decadal predictability.

This article is based on the upcoming article

Kim, H.M., P.J. Webster, and J.A. Curry, 2012: Evaluation of short-term climate change prediction in multi-model CMIP5 decadal hindcasts. *Geophys. Res. Lett.*, **39**, L10701, doi:10.1029/2012GL051644.

Additional Reference

Taylor, K.E., R.J. Stouffer, and G.A. Meehl, 2012: An Overview of CMIP5 and the experiment design. *Bull. Amer. Meteor. Soc.*, **93**, doi:10.1175/BAMS-D-11-00094.1.

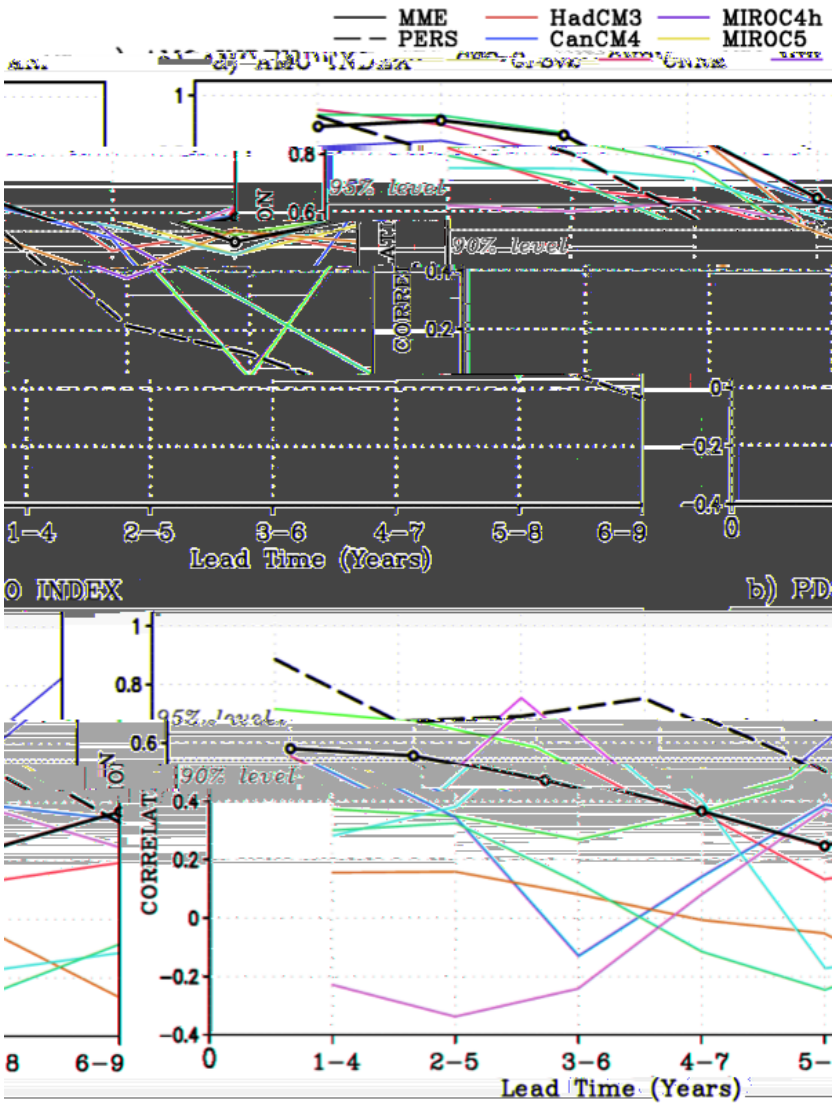

Figure 2. Correlation coefficients for the (a) AMO and (b) PDO index predicted by MME, persistence (PERS) and ensemble-mean of each CMIP5 decadal hindcasts as a function of lead time (years). Solid (dashed) horizontal line represents statistical significance of the correlation coefficients at 95% (90%) confidence level.

U.S. CLIVAR SSC and Panel Membership for 2013

We would like to sincerely thank our Scientific Steering Committee (SSC) members Rob Wood, Annalisa Bracco, and Nick Bond; PSMI Panelists Markus Jochum, David Lawrence, and Joel Norris; and PPAI Panelists Balaji Rajagopalan, Richard Grotjahn, and Gabe Vecchi for their dedicated years of service.

We'd like to welcome new SSC Chair, Bob Weller and Co-Chair, Arun Kumar. Also joining the SSC are Bruce Anderson as PPAI Panel Co-Chair, Tom Farrar as PSMI Panel Co-Chair, and Dimitris Menemenlis as POS Panel Co-Chair.

We also welcome our new Panelists:

Phenomena Observations and Synthesis (POS) Panel

David Halpern (CIT/JPL)
Art Miller (USCD/SIO)
Subrahmanyam Bulusu (USC)

Predictability, Predictions and Applications Interface (PPAI) Panel

Yoo-Geun Ham (NASA/GSFC)
Hyemi Kim (GIT)
Kathy Pegion (NOAA/ESRL)
Andrea Ray (NOAA/ESRL)

Process Study and Model Improvement (PSMI) Panel

Alessandra Giannini (Columbia/IRI)
Jennifer Kay (NCAR)
Aneesh Subramanian (UCSD/SIO)
Lou St. Laurent (WHOI)

The Atlantic Meridional Overturning Circulation (AMOC) in CMIP5 models: RCP and historical simulations

Wei Cheng[1], John Chiang[2], and Dongxiao Zhang[1]
[1]Joint Institute for the Study of the Atmosphere and Ocean, University of Washington, Seattle, Washington
[2]Dept. of Geography and Berkeley Atmospheric Sciences Center, University of California, Berkeley, California

Introduction: The Atlantic Meridional Overturning Circulation (AMOC) produces one of the dominant decadal-multidecadal climate variations in the Earth System, and offers potential for decadal prediction. Full-depth, across-basin measurement of the AMOC is only available from 2004 to the present, through the deployment of the RAPID/MOCHA array (Rayner et al., 2011). State-of-the-art climate models, on the other hand, exhibit a wide range of AMOC behaviors with regard to its mean state and decadal-multidecadal variations. For example, the AMOC variability in pre-industrial control simulations ranges from a 20-30 year oscillation to broad spectral power on the 50-90 year timescale, and with widely varying amplitudes. Indirect observations, mostly paleo proxies, cannot constrain the "true" AMOC variability except to say that both time scales are possible. Moreover, proposed mechanisms of AMOC variations vary substantially, involving ocean dynamics responding to atmospheric stochastic forcing, and/or ocean-atmosphere coupled dynamics. Some models "switch" from one type of behavior to another readily as parameterizations or model components are changed, suggesting that the AMOC variations are determined by a balance of multiple mechanisms, and that this balance varies across models. External forcings – such as anthropogenic greenhouse gases, aerosols, and volcanic eruptions – can similarly force decadal-multidecadal AMOC variations, and the responses are also highly model-dependent. These uncertainties complicate our understanding of the 20th century multidecadal variations, and decadal predictions using climate models.

As part of the community effort to evaluate the new generation climate models used for the IPCC 5th assessment report (AR5), we examined the AMOC simulated by ten Coupled Model Intercomparison Project phase 5 (CMIP5) models for the historical (1850-2005) and future climates. The overturning streamfunctions used to evaluate the AMOC in these models (Table 1) were provided as output by the respective modeling centers. The climate models participating in CMIP5 are more comprehensive than the models participating in the previous intercomparison project (CMIP3); many include interactive biogeochemical components, and prognostic rather than imposed aerosol concentrations. The CMIP5 also made available a large number of ensemble runs for a given scenario; this is necessary to extract possible externally forced AMOC variability, given the strong internal variability of the AMOC. We examined the AMOC mean state and temporal variability, with a focus on understanding the multi-model ensemble mean behavior (Cheng et al., 2012).

Model Names	Historical runs (1850-2005)	RCP4.5 runs		RCP8.5 runs	
		2006 - 2100	2101 - 2300	2006 - 2100	2101 - 2300
CanESM2	5	5	2	5	-
CCSM4	6	5	1	4	-
CNRM-CM5	10	1	-	1	-
GFDL-ESM2M	1	1	-	1	-
MPIESM-LR	3	3	1	3	1
MRI-CGCM3	5	1	-	1	-
NorESM-M	3	1	1	1	-
GFDL-CM3	5	1	-	1	-
NorESM-ME	1	1	-	-	-
MPIESM-P	2	-	-	-	-

Table 1. CMIP5 models used in this study and their numbers of ensemble runs in historical (1850-2005) and RCP simulations. "-" means no run is available under that forcing scenario and time period.

Results - RCP runs: CMIP5 adopted the Representative Concentration Pathways (RCP) for future climate scenarios (Taylor et al., 2012). We analyze simulations for the RCP4.5 (radiative forcing stabilizes at 4.5 W/m2 by 2100) and RCP8.5 (rising radiative forcing leading to 8.5 W/m2 in 2100) scenarios. The AMOC index is defined as the maximum annual mean volume transport streamfunction at 30°N (units: Sv). Of the ten models, eight show a mean value of the AMOC over the 20th century that is within the uncertainty range of the AMOC amplitude measured by the RAPID/MOCHA array (Fig. 1). This may be an improvement relative to the CMIP3 simulations (IPCC, 2007, Fig. 10.15), though it remains to be seen if this holds true once all CMIP5 output becomes available. Under RCP4.5 forcing, all models predict a weakening of the AMOC in the first half of the 21st century (Fig. 1a,c); a majority of the models also show a stabilization of AMOC in the second half of 21st century and subsequent rebound (Fig. 1a,c). In terms of percentage decrease relative to each model's historical average, the magnitude ranges from 5% to 40% by year 2100 under RCP4.5 scenario (Fig. 1c). Under RCP8.5 forcing, all but one model's AMOC decrease to below the low end of present-day observations by 2100 (Fig. 1b), and the percentage decrease ranges from 15% to 60% (Fig. 1d). One model run extends to year 2300 under RCP8.5 forcing; in this model, the AMOC shows stabilization around 2200 and a slight increase thereafter (Fig. 1b). The multi-model mean percentage decrease of the AMOC in the 21st century from CMIP5 is in good agreement with CMIP3 results (e.g., Schmittner et al., 2005).

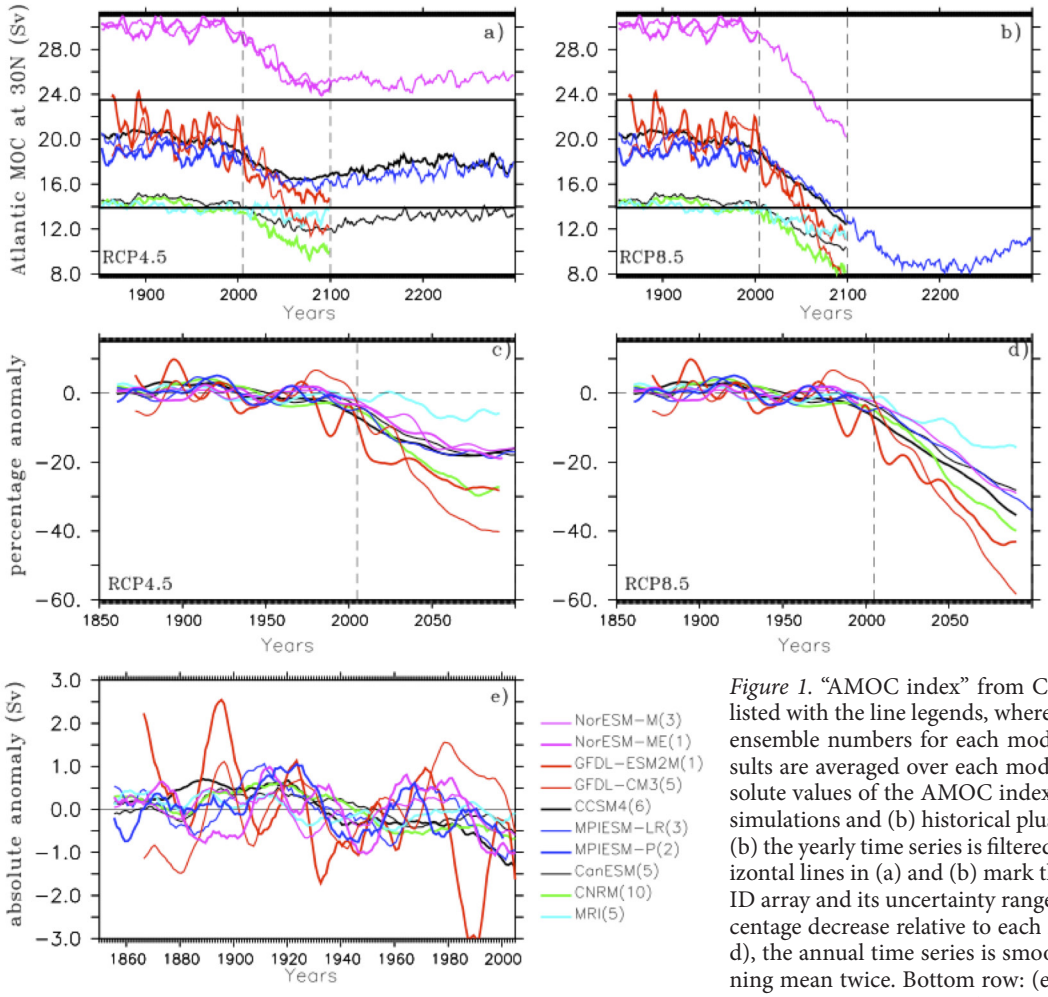

Figure 1. "AMOC index" from CMIP5 models. Model names are listed with the line legends, where numbers in the bracket indicate ensemble numbers for each model's "historical" simulations. Results are averaged over each model's ensemble runs. Top row: absolute values of the AMOC index from (a) historical plus RCP4.5 simulations and (b) historical plus RCP8.5 simulations. In (a) and (b) the yearly time series is filtered by a 5-year running mean. Horizontal lines in (a) and (b) mark the observed AMOC by the RAPID array and its uncertainty range (18.7±4.8 Sv). Middle row: percentage decrease relative to each model's historical average (c and d), the annual time series is smoothed by applying a 11-year running mean twice. Bottom row: (e) absolute AMOC anomalies (in Sv) in years 1850-2005 relative to each model's historical average. The yearly time series in (e) is filtered by a 11-year running mean.

Results - Historical runs: The AMOC anomalies (deviation from each model's historical average) in the 20th century are shown in Fig. 1e. Variability in the AMOC strength typically ranges within ±1Sv of the mean, though the GFDL (GFDL-ESM2M and GFDL-CM3) and MPI (MPIESM-LR and MPIESM-P) models show a stronger multidecadal variation

than other models. The multi-model ensemble mean AMOC anomalies (averaged over 41 ensemble runs) show a multidecadal variation with a period of ~60 years (Fig. 2c) and a peak-to-peak range slightly less than 1 Sv. An EOF analysis combining all model's AMOC timeseries suggests that this multidecadal variation is expressed across all models (Fig. 2). The principal component (PC) of the combined EOF1 represents a downward trend (Fig. 2a), and PC of mode 2 represents a multidecadal variation closely resembling the full AMOC time series (Fig. 2c). All models project onto these leading modes with the same sign, except GFDL-CM3, which shows a strengthening trend over the 20th century (as indicated by its negative eigenvalue in Fig. 2b). The spatial pattern associated with mode 2 is a single cell extending from 75°N to the South Atlantic, with the largest vertical movement anomalies concentrated between 65°N and 45°N. This pattern is similar to results from single model studies.

The multi-model ensemble mean multidecadal AMOC variability is significantly correlated with surface shortwave radiation flux anomalies in the North Atlantic, and with surface freshwater flux anomalies in the subpolar latitudes. If we interpret decadal fluctuations in the net surface shortwave flux anomalies to be caused by external forcing variability (most likely associated with aerosols), then these results suggest a common AMOC response to external climate forcing. Moreover, there is a suggestion that the AMOC response is in sync with the multi-model ensemble mean NAO index, though only in the second half of the 20th century. The AMOC and the NAO indices both show an upward trend from year 1950 to 2000; and, superimposed on this linear trend is

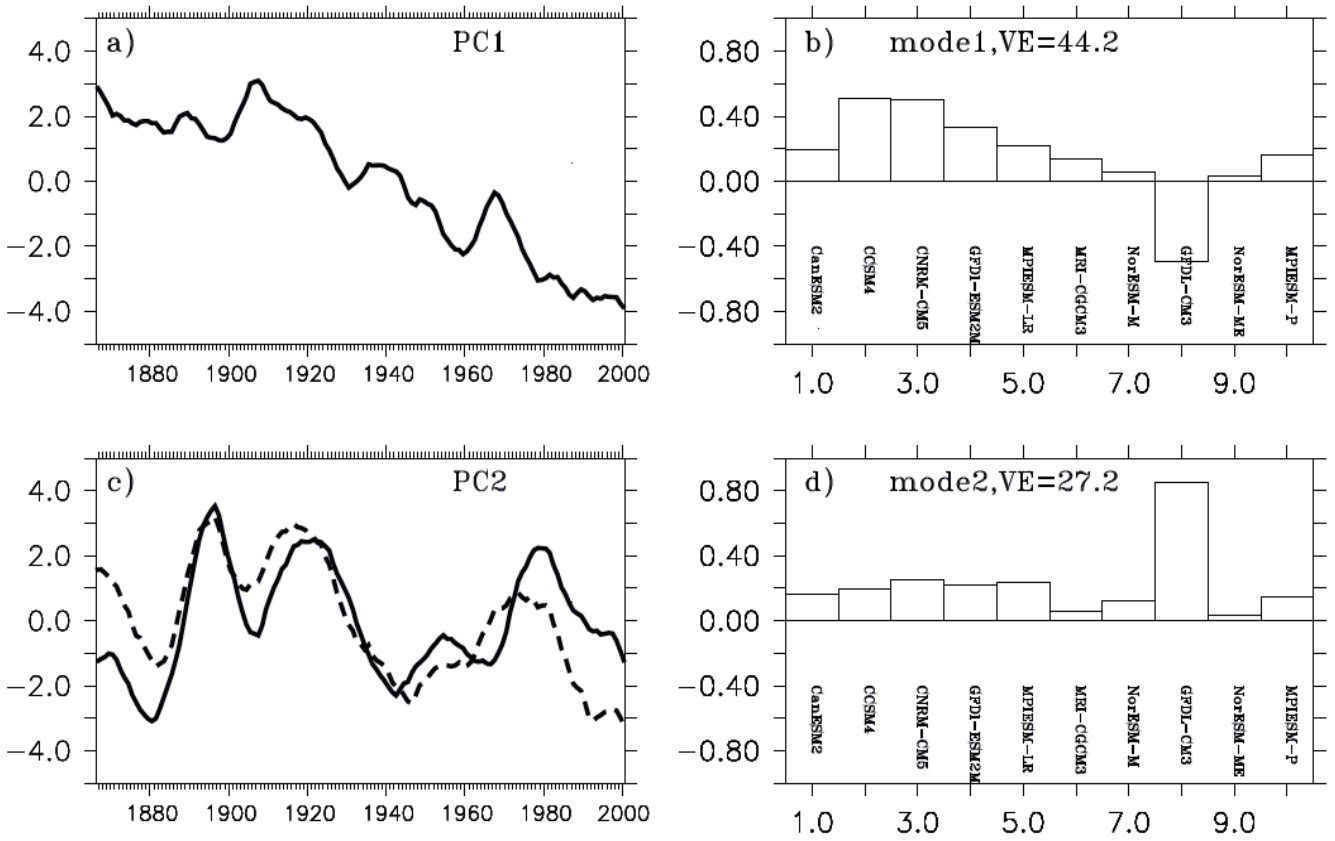

Figure 2. Eigen-value decomposition of multi-model AMOC indices. We multiplied each model's ensemble mean AMOC index anomalies by √N, where N is the number of ensemble runs for each model. The resulting anomalies were combined into a single matrix and eigen-value decomposition was performed on this matrix. The combined EOF modes extract contributions from each model on common principal components across all models. First two principal components (a, c) and eigen-values (b, d) are shown. Variance explained by each mode is marked on the right panels. The dashed line on c) is the original multi-model ensemble mean AMOC anomalies (scaled by a factor of six for displaying purpose).

a multidecadal fluctuation with a maximum around year 1980 (seven out of the ten CMIP5 models demonstrate this temporal characteristic). Finally, the multi-model ensemble mean SST anomalies in the North Atlantic bear temporal resemblance to the observed Atlantic Multidecadal Oscillation (AMO) index, but the amplitude is substantially smaller.

Discussion: The main caveats of the results of this study are the relatively small number of ensemble members used in the analysis, and the relatively wide variety of model responses to similar forcings. The multi-model ensemble mean approach assumes a common external forcing applied across all models; however, the implementation of such 'common' forcings (e.g. anthropogenic aerosols) do vary between different models. Despite these significant uncertainties, our results showing a suggestion of a 'common' AMOC response across models do suggest some hope for understanding the forced AMOC behavior. In the future, more detailed investigation of underlying AMOC mechanisms, and examination of single forcing runs, are required in order to properly detect and attribute the influence of specific forcing agents on the AMOC.

Acknowledgments:

This work was funded by NOAA Climate Program Office as part of CMEP (Coupled Model Evaluation Project). We acknowledge the World Climate Research Programme's Working Group on Coupled Modelling, which is responsible for CMIP, and we thank the climate modeling groups (listed in Table 1 of this paper) for producing and making available their model output.

References

Cheng, W., J.C.H. Chiang, and D. Zhang, 2013: The Atlantic Meridional Overturning Circulation (AMOC) in CMIP5 models: RCP and historical simulations. *J. Climate, in press.*

Rayner, D. et al., 2011: Monitoring the Atlantic meridional overturning circulation. *Deep-Sea Res. II*, **58**, 1744–1753.

Schmittner, A., M. Latif, and B. Schneider, 2005: Model projections of the North Atlantic thermohaline circulation for the 21st century assessed by observations. *Geophys. Res. Lett.*, **32**, doi:200510.1029/2005GL024368.

Taylor, K. E., R. J. Stouffer, and G. A. Meehl, 2012: An Overview of CMIP5 and the Experiment Design. *Bull. Amer. Meteor. Soc.*, **93**, 485–498.

Sahel rainfall trends in CMIP5 models

Michela Biasutti
Columbia University/Lamont-Doherty Earth Observatory

The origin of the 20th century drought in the Sahel, the semi-arid region to the south of the Sahara, has been hotly debated. Local land and vegetation processes were first thought to be the key mechanism for drought (Charney, 1975), but have since been shown to be secondary to the influence of sea surface temperature (SST) anomalies. Land processes can play a substantial role in modulating and lengthening the drought (Zeng et al., 1999; Kucharsky et al., 2012), but tropical SST variations are the essential forcing (for example, Folland et al., 1986; Giannini et al. 2003; Biasutti et al 2008).

Given the undisputable anthropogenic influence on surface anomalies, recent research has investigated whether the bulk of the Sahel drought resulted from anthropogenic increases in greenhouse gases and aerosols (e.g. Biasutti and Giannini, 2006), or whether it resulted from natural oceanic variability (e.g. Ting et al, 2009). A confident attribution remains elusive. This is due in part to concerns about model biases in climatology and variability (e.g. Cook and Vizy, 2006), in part to the widely different response of the CMIP3 coupled models to greenhouse gas forcing (e.g. Biasutti et al., 2008; Patricola and Cook, 2009; Giannini 2010).

Our work under the aegis of the Climate Model Evaluation Project suggests that the CMIP5 models are still lacking the ability to fully capture multi-decadal swings in Sahel rainfall, but progress has been made in the sense that there is better agreement in future rainfall projections.

At the centennial timescale (Figure 1c), the observed trends fall well within those in the historical simulations,

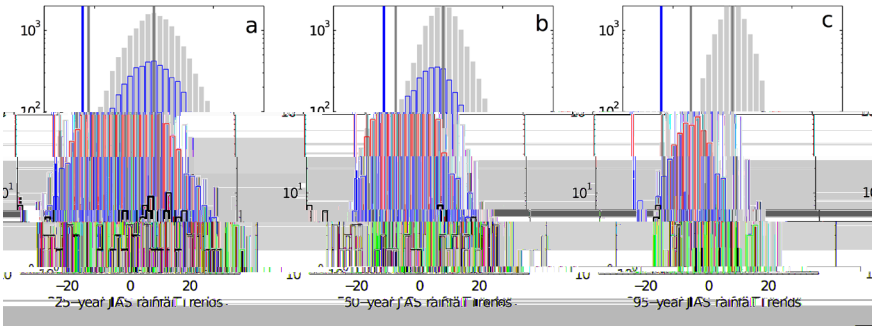

Figure 1. Distributions of 25-year (left), 50-year (center) and 95-year (right) trends in pre-industrial (gray) and historical (blue) integrations and in the observations (black; thicker line is for the Hulme dataset, thinner line for TS3p1, both from the University of East Anglia Climate Research Unit). Running windows over the available period in each integration and observations were used to calculate the individual trends. Histograms are not normalized and are plotted on a semi-log scale to emphasize the low counts. The gray and blue lines to the left in each plot indicate the one-in-a-hundred trend in the pre-industrial and historical simulations and help put the observed trends in context. The zero value is highlighted by a vertical gray bar.

but they appear as a very rare event in the pre-industrial integrations. This result confirms that the long term drying of the Sahel was in part anthropogenically driven. However, even at these long time scales, the anthropogenic effect (as estimated from the ensemble mean of the historical simulations) is only about a 5% reduction in rainfall--about a quarter of the observed 20th century trend. For comparison, Biasutti and Giannini (2006) had estimated from CMIP3 an anthropogenic contribution of about a third.

A linear trend is, in any case, a poor portrait of the observed Sahel time series, with its large multi-decadal oscillations. At these timescales (Figure 1a, b), the distributions suggest that the models are biased and incapable of reproducing the observed variability. Booth et al. (2012) suggest that most CMIP5 models underestimate the strength of the indirect aerosol forcing, but this conclusion might be premature (Zhang et al. 2013). It is possible that the models' deficiencies are due to poor representation of relevant ocean/atmosphere coupled dynamics (Rowell, 2013), or missing land processes (Kucharsky et al., 2012; Yoshioka et al., 2007). Keeping these caveats in mind, we now turn to the 21st century projections. Their most robust aspects are summarized in Figure 2: The CMIP5 models project a rainy season that is feebler at its start, especially in West Africa, and more abundant at its core and end. Out of 20 models, only 4 buck this consensus. CMIP3 already suggested both a shift in seasonality and a distinction between West Africa and the rest of the Sahel (see, for example, Biasutti and Sobel, 2009, Caminade and Terray, 2010). The consistency between CMIP3 and CMIP5 leads us to put more faith in the new projection. However, there is still a large spread in the magnitude, if not the sign, of the early- and late-season projections and outlier models persist. Moreover in large swaths of the Sahel the projections for seasonal totals (dominated by anomalies in the core rainy season) remain uncertain even in sign.

CMIP5 idealized simulations (Taylor et al., 2012) can help us understand the mechanisms responsible for the scenario anomalies. We use simulations forced by a steady increase in CO_2 concentration (1% to 4x) and others that distinguish the fast response of the land-atmosphere system to the CO_2 increase (before the ocean adjusts, 4x SST clim) from the slow response due to the eventual changes in SST (Abrupt 4x). Results are shown in Fig. 3.

Forcing by increasing CO_2 is sufficient to reproduce the scenario anomalies in the Sahel: an indication that additional forcings from aerosols play a negligible role in determining the mean response in the 21st century scenario simulations. However, the full response is not captured as a simple superposition of the fast and

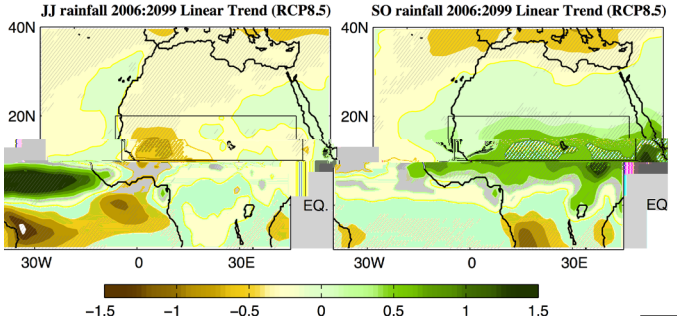

Figure 2. RCP8.5 trends in Sahel rainfall in the multi-model mean for the onset season (June and July, left) and the demise season (September and October, right). Maps are in mm/day and are the difference between the end points of the linear trend over 2006:2099. The mean of available ensemble runs is used for each model (using 20 models). Stippling indicates grid boxes where 15 or more of the models produced either a positive or a negative trend.

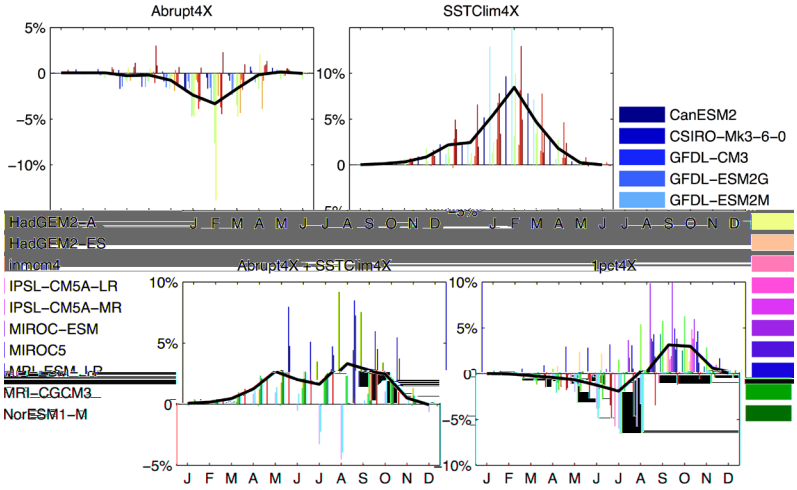

Figure 3. Annual cycles of Sahel rainfall changes in idealized runs capturing the fast and slow response to CO_2 and the combined effects. Top left: Anomalies due to SST (slow response) are calculated as long- term trends in the Abrupt4xCO_2 runs. Top right: Anomalies due to CO_2 (fast response) are calculated as the difference between the SSTClim4xCO_2 and SSTClim runs. Bottom left: the linear combined effect of CO_2 and SST is calculated as the sum of the top panels. Bottom right: the full effect of quadrupling CO_2 is calculated as the trend over 140 years integrations with CO_2 growing by 1% per year. Units are in percentage of total annual rainfall. Models are color coded as in the legend, but not all models are present in all panels.

slow response to CO_2. The effect of CO_2 alone (without SST warming) is to induce wetting in the Sahel, while warmer SSTs induce drying (see also Patricola and Cook, 2010). In isolation, each of these two forcings produce rainfall anomalies that peak in August, at the peak of the rainy season, and their sum does not yield early season drying and late season wetting. (The effect of SST is largest, at least in the mean, and the sum of the rainfall anomalies is positive year round). It is only when the direct CO_2 forcing and the SST warming can interact in a fully coupled system (1% to 4x) that they give rise to the change in seasonality seen in the scenario simulations. We speculate that the mutual influences of land and ocean and the inherent difference in the phase and amplitude of their annual cycle are important to determine the projected delay of the Sahel rains in the coupled response.

References

Biasutti, M., 2013: Forced Sahel rainfall trends in the CMIP5 archive. *J. Geophys. Res.*, **118**. doi:10.1002/jgrd.50206.

Biasutti, M., and Giannini, A., 2006: Robust Sahel drying in response to late 20th century forcings. *Geophys. Res. Lett.*, **33**. doi:10.1029/2006GL026067.

Biasutti, M., and Sobel, A. H., 2009: Delayed seasonal cycle and African monsoon in a warmer climate. *Geophys. Res. Lett.* **36**, L23707. doi:10.1029/2009GL041303.

Biasutti, M., Held, I. M., Sobel, A. H., and Giannini, A., 2008: SST forcings and Sahel Rainfall Variability in Simulations of the Twentieth and Twenty-First Centuries. *J. Climate*, **21**, 3471–3486.

Booth, B. B. B., Dunstone, N. J., Halloran, P. R., Andrews, T., and Bellouin, N. (2012). Aerosols implicated as a prime driver of twentieth-century North Atlantic climate variability. *Nature*, **484**, 228–232. doi:10.1038/nature10946.

Caminade, C., and Terray, L., 2010: Twentieth century Sahel rainfall variability as simulated by the ARPEGE AGCM, and future changes. *Climate Dyn.*, **35**, 75–94. doi:10.1007/s00382-009-0545-4.

Charney, J. G., 1975: Dynamics of deserts and drought in the Sahel. *Quart. J. Roy. Meteor. Soc*, **101**, 193–202.

Cook, K. H., and Vizy, E. K., 2006: Coupled model simulations of the West African monsoon system: 20th and 21st century simulations. *J. Climate*, **19**, 3681–3703. doi:10.1175/JCLI3814.1.

Folland, C. K., Palmer, T. N., and Parker, D. E., 1986: Sahel rainfall and worldwide sea temperature. *Nature*, **320**, 602–687.

Giannini, A., 2010: Mechanisms of Climate Change in the Semiarid African Sahel: The Local View. *J. Climate*, **23**, 743–756.

Giannini, A., Saravanan, R., and Chang, P., 2003: Oceanic forcing of Sahel rainfall on interannual to interdecadal time scale. *Science*, **302**, 1027–1030.

Kucharski, F., Zeng, N., and Kalnay, E., 2012: A further assessment of vegetation feedback on decadal Sahel rainfall variability. *Climate Dyn*. doi:10.1007/s00382-012-1397-x.

Patricola, C. M., & Cook, K. H. (2009). Northern African climate at the end of the twenty-first century: an integrated application of regional and global climate models. *Climate Dyn.*, **35**, 193–212. doi:10.1007/s00382-009-0623-7.

Patricola, C. M., & Cook, K. H., 2010: Sub-Saharan Northern African climate at the end of the twenty-first century: forcing factors and climate change processes. *Climate Dyn.*, **37**, 1165–1188. doi:10.1007/s00382-010-0907-y.

Rowell, D. P., 2013: Simulating SST Teleconnections to Africa: What is the State of the Art? *J. Climate*. doi:10.1175/JCLI-D-12-00761.1.

Taylor, K. E., Stouffer, R. J., and Meehl, G. A., 2012: An Overview of CMIP5 and the Experiment Design. *Bull. Amer. Meteor. Soc.*, **93**, 485–498. doi:10.1175/BAMS-D-11-00094.1.

Ting, M., Kushnir, Y., Seager, R., and Li, C. , 2009: Forced and Internal Twentieth-Century SST Trends in the North Atlantic. *J. Climate*, **22**, 1469–1481. doi:10.1175/2008JCLI2561.1.

Yoshioka, M., Mahowald, N. M., Conley, A. J., Collins, W. D., Fillmore, D. W., Zender, C. S., and Coleman, D. B., 2007: Impact of Desert Dust Radiative Forcing on Sahel Precipitation: Relative Importance of Dust Compared to Sea Surface Temperature Variations, Vegetation Changes, and Greenhouse Gas Warming. *J. Climate*, **20**, 1445–1467. doi:10.1175/JCLI4056.1.

Zeng, N., Neelin, J. D., Lau, K. M., and Tucker, C. J., 1999: Enhancement of interdecadal climate variability in the Sahel by vegetation interaction. *Science*, **286**, 1537–1540.

Zhang, R., Delworth, T. L., Sutton, R., Hodson, D. L. R., Dixon, K. W., Held, I. M., et al., 2013: Have Aerosols Caused the Observed Atlantic Multidecadal Variability? *J. Atmos. Sci.* doi:10.1175/JAS-D-12-0331.1.

Multiannual-to-decadal variability of the American monsoons: present climate and CMIP5 projections

Leila M. V. Carvalho and Charles Jones
University of California, Santa Barbara

The presence of a monsoonal type of circulation involving intense convective activity and heavy precipitation is the dominant climatic feature in the tropical Americas during the respective summer seasons. The North American monsoon system (NAMS) and the South American monsoon system (SAMS) are often interpreted as the two extremes of the seasonal cycle of heat, moisture transport and precipitation over the Americas (Vera et al. 2006). The SAMS and NAMS seasonal cycles are essentially driven by the differential heating between the continent and ocean. The global mean concentration of carbon dioxide and associated atmospheric radiative forcing has dramatically increased in the last decades (Foster et al. 2007). Changes in atmospheric forcing modify the distribution of the atmospheric heating altering ocean-continent contrasts with consequences to the monsoon circulation and hydrological cycle. The atmospheric moisture content increases in response to global warming following the Clausius-Clapeyron relationship, but the rate of precipitation increase is slower as predicted by climate models (Held and Soden 2006). Model results and future scenarios of climate change indicate that rainfall tends to increase in convergence zones with large climatological precipitation and to decrease in regions with subsidence (e.g., Chou and Neelin 2004). The availability of the fifth phase of the Coupled Model Intercomparison Project (CMIP5) simulations provided invaluable data sets to further investigate the future projections of climate change in American monsoon regions.

Carvalho and Jones (2013) investigated multiannual changes in the 850hPa temperature (T850), specific humidity (Q850) and daily precipitation over SAMS and NAMS using the National Centers for Environmental Prediction/National Center for Atmospheric Research (2.5o lat/lon grid spacing and during 1 January 1948 to 31 December 2010- hereafter NCEP/NCAR) (Kalnay et al. 1996), the Climate Forecast System Reanalysis (0.5o lat/lon grid spacing during 1 January 1979-31 December 2010 - CFSR) (Saha et al. 2010) and the CMIP5 simulations for two scenarios: "historic" and high emission representative concentration pathways "RCP8.5". Trends in the magnitude and area of the 85th percentiles were distinctly examined over North America (NA) and South America (SA) during the peak of the respective monsoon season.

The historic simulations (1951-2005) and the two reanalyses agree well and indicate that significant warming has already occurred over tropical SA with a remarkable increase in the area and magnitude of the 85th percentile in the last decade (1996-2005). The warming is more extensive over eastern Brazil in the region formerly occupied by savanna, which has been consistently replaced by crops and pasture. In contrast the 85th percentile of T850 and Q850 has not significantly increased over the NAMS domain during the 1996-2005 period.

The RCP8.5 CMIP5 ensemble mean projects an increase in the T850 85th percentile of about 2.5oC by 2050 and 4.8oC by 2095 relative to 1995 over SA (Fig. 1, top). Over NA, the projected change is 2.8oC by 2050 and 5.5oC by 2095 relative to 1955 (Fig. 2, top). The area of SA (NA) that is observed with T850 ≥ the 85th percentile is projected to increase from ~10% (15%) in 1955 to ~58% (~33%) by 2050 and ~80% (~50%) by 2095. The respective increase in the 85th percentile of Q850 is about 3g/kg over SAMS and NAMS by 2095. CMIP5 models project variable changes in daily precipitation over tropical Americas. The most consistent is increased rainfall in the intertropical convergence zone in DJF (Fig. 1) and JJA and decreased precipitation over NAMS in JJA (Fig. 2).

Jones and Carvalho (2013) examined the large-scale characteristics of the SAMS seasonal amplitudes, onset and demise dates, duration and total seasonal precipitation (from the onset to the demise). Changes in the SAMS were investigated with gridded precipitation, CFSR reanalyses and CMIP5 simulations for the "historic"

and "RCP8.5" scenario. Qualitative comparisons with a previous study indicate that some CMIP5 models have significantly improved their representation of the SAMS relative to their CMIP3 versions. In contrast, some models exhibit persistent deficiencies in simulating the SAMS. CMIP5 model simulations for the historical experiment show signals of climate change in South America. While the observational data show trends, the period used is too short for final conclusions concerning climate change.

Future changes in the SAMS were analyzed with six CMIP5 model simulations of the RCP8.5 high emission scenario. Most of the simulations show significant increases in seasonal amplitudes, early onsets, late demises and durations of the SAMS. The simulations for this scenario project a 30% increase in the amplitude from the current level by 2045-2050. In addition, the RCP8.5 scenario projects an ensemble mean 14-day decrease in the onset and 17-day increase in the demise date of

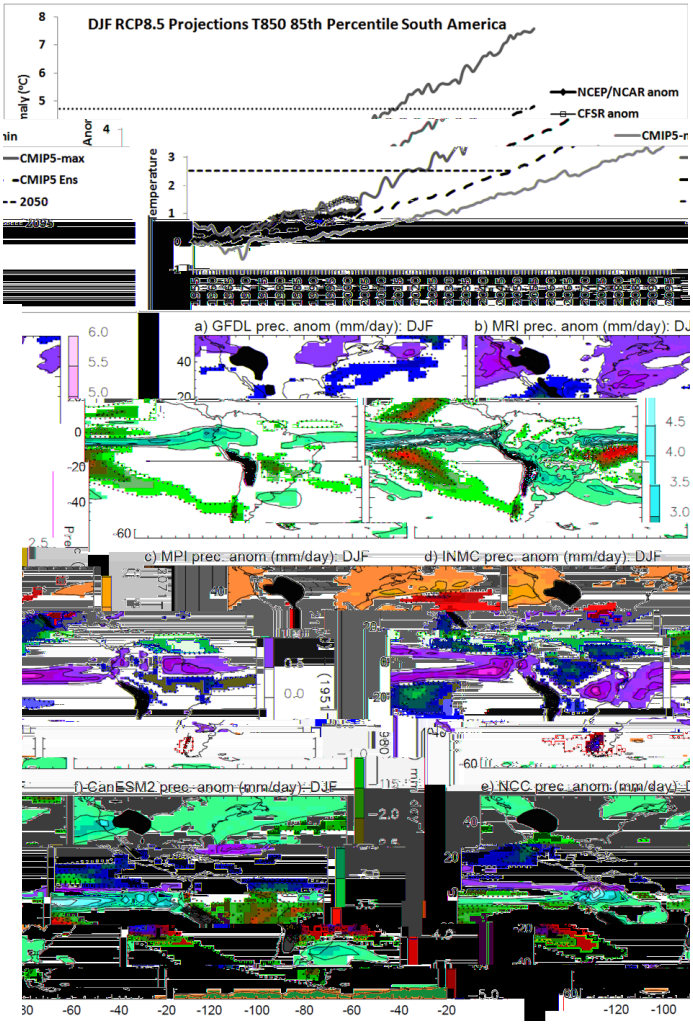

Figure 1. (Top) a) CMIP5 historic simulations and RCP8.5 ensemble mean, maximum and minimum projections of T850p85 anomalies (intercept of the linear fit removed) over SA during DJF. (Bottom) Difference in daily mean precipitation (mm day-1) during DJF between the following 30-yr periods: 2071 to 2100 (RCP85) minus 1951-2005 (historic simulation). Only differences above (below) 0.5 (-0.5) mm day-1 are shown. Dotted (solid) lines indicate negative (positive) anomalies and are plotted every 1mm day-1: a) GFDL-ESM2M, b) MRI-CGCM3, c) MPI-ESM-LR, d) INM-CM4, e) NorESM1-M, f) CanESM2. Dark gray shade indicates topography above 1500m.

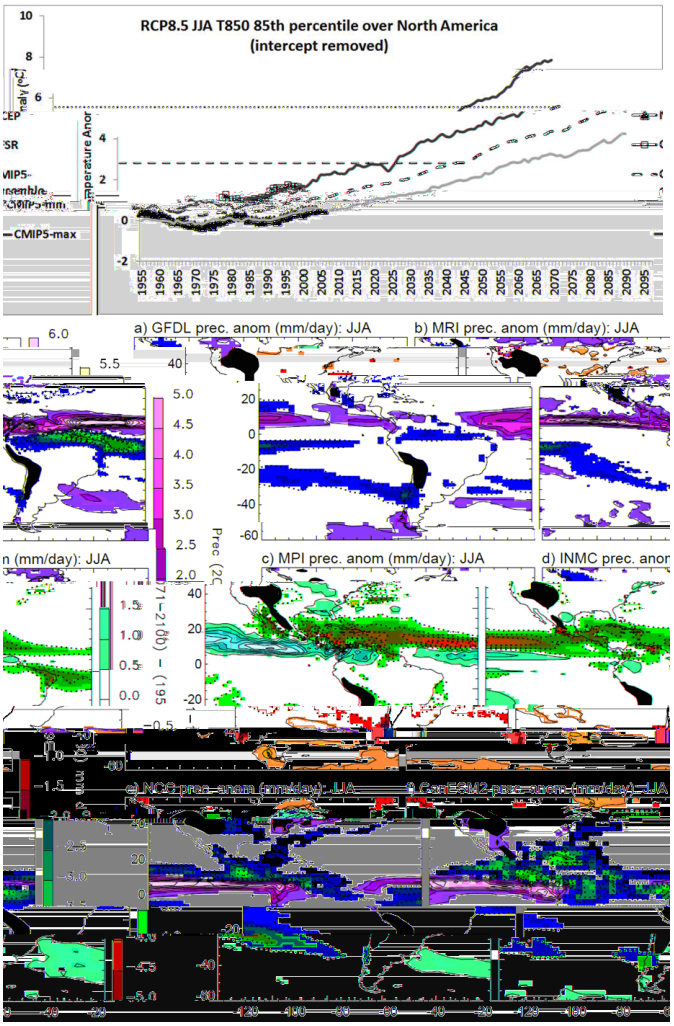

Figure 2. (Top) a) CMIP5 historic simulations and RCP8.5 ensemble mean, maximum and minimum projections of T850p85 anomalies (intercept of the linear fit removed) over NA during JJA. (Bottom) The same as Fig. 1 but for JJA.

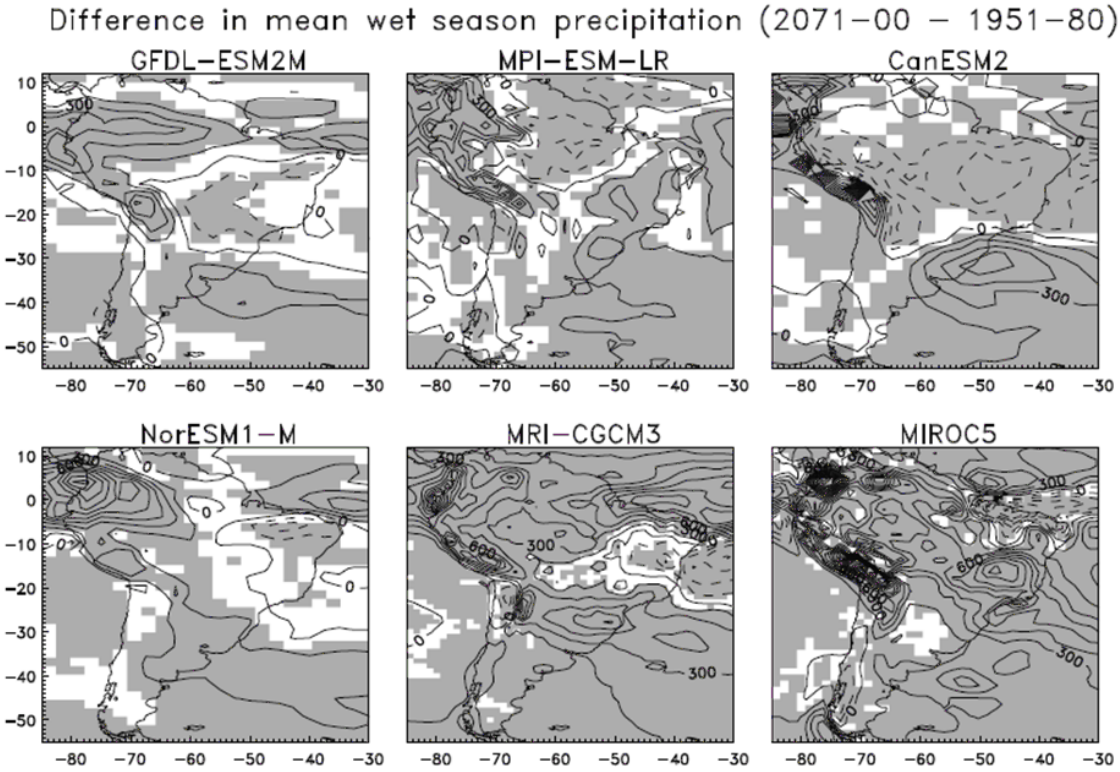

Figure 3. Difference between mean total wet season precipitation during 2071-2100 and 1951-1980. Wet season precipitation is computed as the total from onset to demise dates of SAMS and average during 2071-2100 and 1951-1980. Solid (dashed) lines indicate positive (negative) values (150 mm day-1 interval). Shaded regions are statistically significant at 5% level. Note: MIROC difference is computed between MIROC5 and MIROC4h.

the SAMS by 2045-2050. Additionally, there is a lack of spatial agreement in model projections of changes in total wet season precipitation over SA during 2070-2100. The most consistent CMIP5 projections are the increase in the total monsoon precipitation over southern Brazil, Uruguay and northern Argentina.

Acknowledgments: This study was supported by NOAA Climate Program Office Modeling, Analysis, Predictions and Projections (MAPP) Program as part of the CMIP5 Task Force (grant NA10OAR4310170) and the National Science Foundation RAPID program (grant AGS-1126804). This research was conducted under the CGIAR Research Program on Climate Change, Agriculture and Food Security (CCAFS) and benefited from a sub-contract with the International Potato Center in Lima, Peru (SB120184). We acknowledge the World Climate Research Programme Working Group on Coupled Modeling, which is responsible for CMIP, and we thank the climate modeling groups that provided the CMIP5 models.

References

Carvalho, L. M. V., and Jones, C., 2013: CMIP5 simulations of low-level tropospheric temperature and moisture over tropical Americas. *J. Climate* (Accepted).

Chou C., and J. D. Neelin, 2004: Mechanisms of global warming impacts on regional tropical precipitation. *J. Climate* **17**, 2688–2701.

Forster P, and co-authors, 2007: Changes in atmospheric constituents and in radiative forcing. In: Solomon S, Qin D, Manning M, Chen Z, Marquis M, Averyt KB, Tignor M, Miller HL (eds) Climate change 2007: the physical science basis. contribution of working group I to the fourth assessment report of the intergovernmental panel on climate change. Cambridge University Press, Cambridge.

Held, I. M. and B. J. Soden, 2006: Robust Responses of the Hydrological Cycle to Global Warming. *J. Climate*, **19**, 5686-5699.

Jones, C., and L. M. V. Carvalho, 2013: Climate change in the South American Monsoon System: present climate and CMIP5 projections. *J. Climate* (Accepted).

Kalnay, E., and Co-authors, 1996: The NCEP-NCAR 40 Year Reanalysis Project. *Bull. Amer. Meteor. Soc.,* **77**, 437-471.

Saha, S., and Co-authors, 2010: The NCEP Climate Forecast System Reanalysis. *Bull. Amer. Meteor. Soc.*, **91**, 1015-1057.

Vera and co-authors, 2006: Toward a unified view of the American monsoon systems. *J. Climate*, **19**, 4977–5000.

Evaluation of multidecadal variability in CMIP5 surface solar radiation and inferred underestimation of aerosol direct effects over Europe, China, Japan and India

Robert J. Allen[1], Joel R. Norris[2], and Martin Wild[3]
[1]Department of Earth Sciences, UC Riverside, Riverside CA
[2] Scripps Institution of Oceanography, UC San Diego, San Diego CA
[3] Institute for Atmospheric and Climate Science, ETH Zurich, Switzerland

Solar radiation incident upon the surface of the Earth plays a critical role in the climate system, driving surface temperatures, large-scale atmospheric circulation, and the hydrological cycle, while also of extreme importance to the biosphere. Measurements in many regions throughout the world have shown large multidecadal swings in all sky surface solar radiation, with decreases throughout the 1950s-1980s ("dimming") and increases during the 1990s ("brightening") (e.g., Ohmura and Lang, 1989; Gilgen et al., 1998; Wild 2009). These variations in surface solar radiation are consistent with several independent observations, including sunshine duration, diurnal temperature range, and pan evaporation.

Prior studies have shown global climate models generally simulate the observed dimming/brightening qualitatitvely, but underestimate the corresponding magnitude over several regions (e.g., Ruckstuhl and Norris, 2009; Dwyer et al., 2010; Wild and Schmucki, 2011). In support of the upcoming IPCC fifth assessment report, the newest model intercomparion project, CMIP5 (Taylor et al., 2012), is now underway. Since most CMIP5 models contain an improved representation of aerosols, it is of interest to evaluate the ability of CMIP5 models to simulate the observed dimming and brightening trends. Models that exhibit the observed magnitude and timing of dimming/brightening likely have more realistic aerosol radiative forcing, more accurate estimates of climate sensitivity, and better regional and global scale climate simulations and projections.

Monthly downwelling all sky and clear sky surface solar radiation, total cloud cover and several aerosol fields, such as absorption aerosol optical depth (AAOD) at 550 nm, were downloaded for all available CMIP5 models. This resulted in a total of 42 climate models and 173 realizations. Observed monthly mean values of all sky surface solar radiation were obtained from the Global Energy Balance Archive (GEBA; Gilgen and Ohumura, 1999) for Europe, China, India, and Japan. We calculated time series of regional mean anomalies in observed and modeled downwelling flux. Each CMIP5 variable was interpolated to the same grid boxes used for the observations, for each region.

Because GEBA data are for all sky conditions, they include the radiative effects of cloud cover. Following Norris and Wild (2007), we used surface and satellite measurements of cloud cover to empirically remove cloud cover radiative effects from the GEBA all-sky radiation flux. The resulting quantity, called "clear sky proxy" radiation, includes both clear sky radiation anomalies and the effects of changes in cloud albedo that are uncorrelated with cloud cover. The use of clear sky proxy anomalies allows the radiative effects of long-term changes in anthropogenic aerosol to be more clearly distinguished from natural weather (i.e., clouds) and climate variability. CMIP5 clear sky proxy anomalies are calculated in a similar manner.

Figure 1 shows the time series of clear sky proxy annual mean anomalies over each region for both observations and models. The right hand panels show scatterplots of the corresponding dimming and brightening trends. Since solar dimming over Europe occurs prior to ~1990, we choose the 1971-1986 and 1987-2007 time periods for trend calculations (results are not sensitive to the exact choice of transition year). Models as a whole significantly underestimate the decrease in surface solar radiation over 1971-1986. In terms of individual model realizations, none reproduce the magnitude of the observed dimming (although 95% confidence ranges overlap), with the largest decrease in clear sky proxy radiation about half that observed. The observed increase

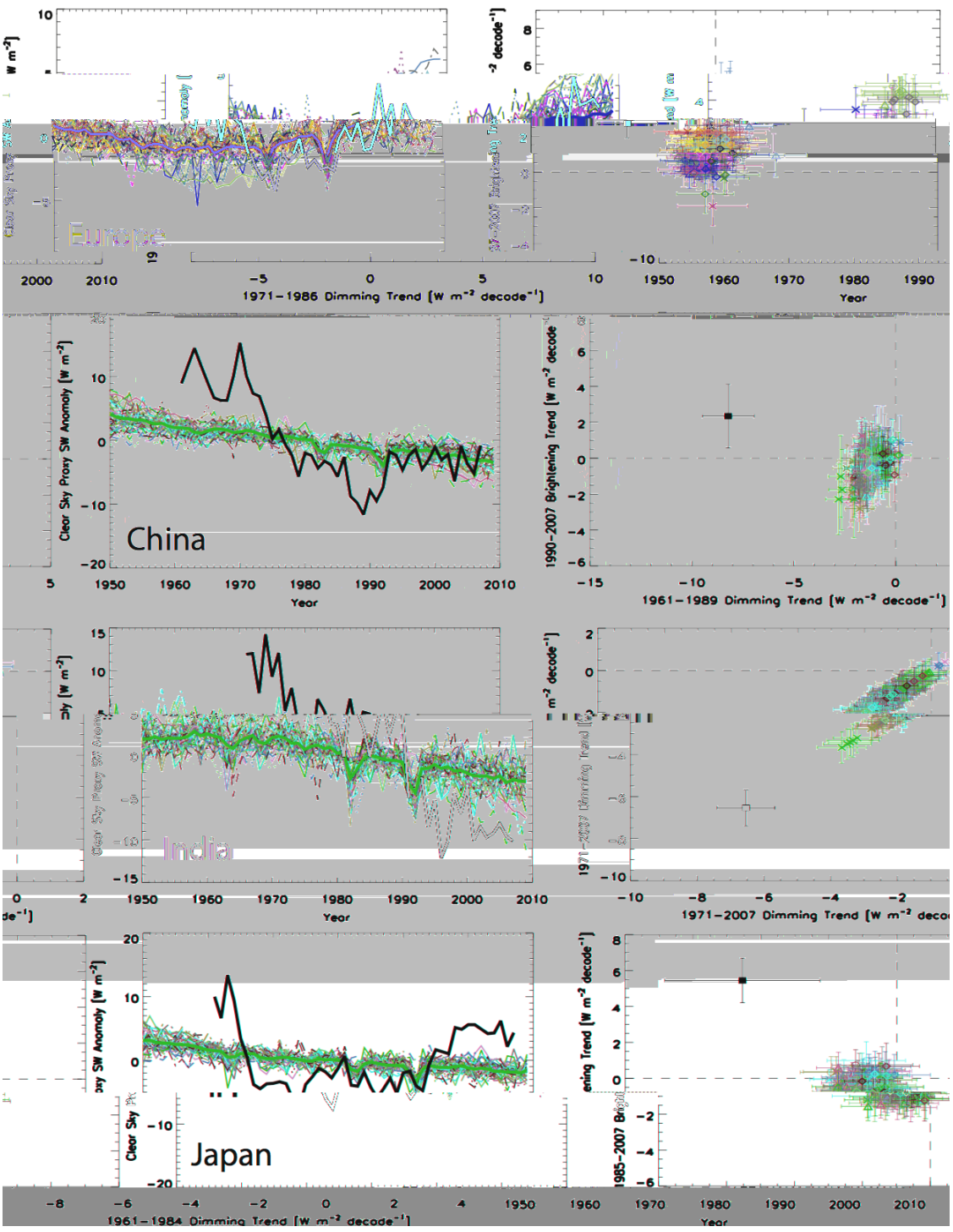

Figure 1. Clear sky proxy annual mean anomaly time series (left) and scatter plots of the dimming versus the brightening trend (right) for Europe (top), China (middle top), India (middle bottom) and Japan (bottom). The left panels show the model-mean time series for each model, with the CMIP5 ensemble mean in thick red; scatter plots show each model- realization. Observations are in black. Error bars show the 95% confidence interval of the trend, accounting for autocorrelation. Clear sky proxy units are W m−2, with trend units of W m−2 decade−1.

in European clear sky proxy radiation over 1987-2007 is also underestimated by the CMIP5 mean, but this is not significant at the 95% confidence level. In fact, some individual models simulate the magnitude of the observed brightening, with CNRM-CM5 (blue circle) and MIROC5 (gray diamond) actually overestimating the brightening.

Observations over China show a large decrease in clear sky proxy radiation from 1961-1989, followed by a much weaker recovery, most of which occurs during the early 1990's. CMIP5 shows a significant decrease during the observed dimming time period and a nonsignificant decrease during the brightening time period. Thus, the CMIP5 ensemble mean simulates the observed dimming over 1961-1989, but significantly less than observed. The ensemble mean

also simulates continued dimming during the 1990-2007 time period, in disagreement with observations. The largest dimming trend of a single realization is less than half of that observed, by GFDL-CM3 (red X). However, GFDL-CM3, as well as other models that yield the largest dimming trends (e.g., CSIRO-Mk3-6-0), also yield continued dimming during 1990-2007, when observations suggest a recovery.

Unlike Europe and China, observations show that India does not exhibit a recovery in clear sky proxy radiation. A large decrease in clear sky proxy radiation occurs throughout 1971-2007. The corresponding CMIP5 ensemble mean trend is also negative, but significantly less than observed. Similar to China, GFDL-CM3 (red X) yields the largest decrease in clear sky proxy radiation over India. However, this is about 50% of the observed trend, and significantly less.

The last region we consider, Japan, exhibits a large decrease in clear sky proxy radiation during the first 10-15 years, followed by a relatively stable period from the mid-1970s to ~1990, which in turn is followed by a recovery. Using 1984/85 as the transition year, observed clear sky proxy anomalies yield significantly more dimming and brightening than the corresponding CMIP5 ensemble mean dimming and brightening trends. Similar to China, the CMIP5 ensemble reproduces the observed dimming but significantly underestimates the magnitude, and continues to simulate dimming during the brightening time period. The scatter plot shows no model realization is able to reproduce the magnitude of the observed dimming and brightening trends over Japan. There are several reasons why CMIP5 models may underestimate the magnitude of the observed dimming and brightening. Because aerosol direct effects appear to be the primary drivers of dimming and brightening, possible sources of error include 1) aerosol emissions do not increase/decrease enough; 2) modeled aerosol loads (which involve simulation of transport, aging, and deposition) do not increase/decrease enough; 3) models neglect important aerosol species and 4) models are not sensitive enough to aerosols (i.e., deficient scattering and absorption of solar radiation). Similarly, incorrect simulation of the sign of observed changes in surface solar radiation (e.g., brightening over China and Japan) is likely related to lack of, or incorrect timing

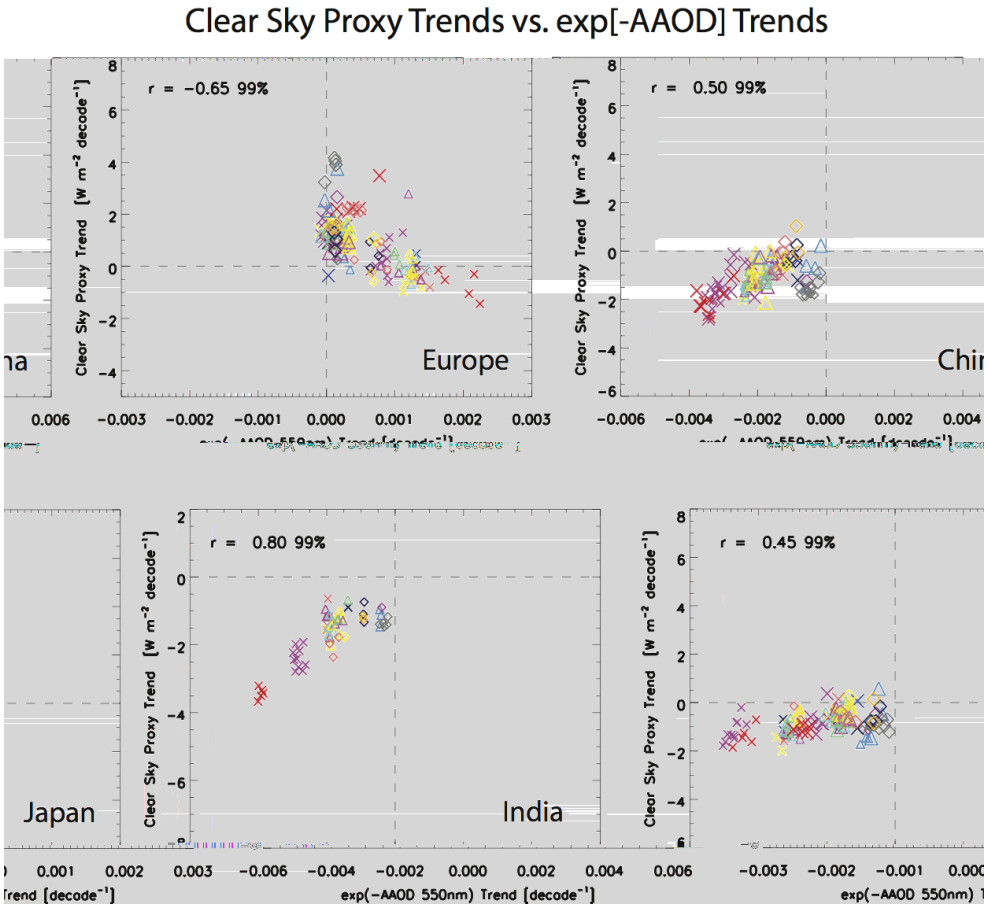

Figure 2. Scatter plots of annual mean clear sky proxy trends versus exp[-AAOD 550nm] trends during the dimming (smaller symbols) and brightening (larger symbols) periods for each of the four regions. The correlation coefficient and the corresponding significance level is included in each panel. Only models with archived aerosol data are included.

of, a transition from increasing to decreasing aerosol emissions.

CMIP5 underestimation of the European dimming appears to be largely due to the emissions inventory, which shows decreasing aerosol emissions over the entire 1971-1986 dimming time period (not shown). Reasons for model underestimation of the dimming over China, Japan, and India are less certain, but may be due to underestimation of black carbon (BC) solar absorption and/or underestimation of the increase in BC emissions. Figure 2 shows that all three regions possess relatively large inter-model correlations between exp[-AAOD 550nm] trends and clear sky proxy trends, at 0.45 for Japan, 0.50 for China, and 0.80 for India (the negative European correlation appears to be related to an inverse relationship between modeled sulfate and BC trends, and the dominance of sulfate in driving European dimming/brightening). This relationship is the strongest of any of the aerosol-clear sky proxy relationships we evaluated for both India and Japan. Trends in exp[-AAOD 550nm] also correlate well with BC load trends, ranging from 0.61 over India to 0.75 over Japan. Moreover, the CMIP5 models that simulate the largest dimming over China and India (GFDL-CM3 and CSIRO-Mk3-6-0) possess the largest increase in AAOD.

Additional support for deficient BC forcing comes from the fact most climate models underestimate BC solar absorption by a factor of almost three (Bond et al., 2013 and references therein). Models also underestimate BC surface concentrations (Koch et al., 2009) and aerosol optical depth (Chung et al., 2012). Similarly, Atmospheric Chemistry CMIP models, eight of which are included in CMIP5, strongly underestimate present-day AAOD over four regions, including China and India (Shindell et al., 2012). Underestimation of aerosol radiative effects will not only impact the simulated climate in these regions, but may also affect the simulation of large-scale atmospheric circulation, such as the recent widening of the tropical belt (Allen et al., 2012). Additional work is necessary to better understand why models underestimate Chinese, Indian and Japanese dimming, and the corresponding consequences to simulated regional and global climate.

References

Allen, R. J., S. C. Sherwood, J. R. Norris, and C. S. Zender, 2012: Recent Northern Hemisphere tropical expansion primarily driven by black carbon and tropospheric ozone. *Nature*, **485**, 350–354.

Bond, T. C., S. J. Doherty, D. W. Fahey and et al., 2013: Bounding the role of black carbon in the climate system: A scientific assessment. *J. Geophys. Res.*, doi: 10.1002/jgrd.50171.

Chung, C. E., V. Ramanathan, and D. Decremer: 2012: Observationally constrained estimates of cabonaceous aerosol radiative forcing. *Proc. Natl. Acad. Sci.*, doi:10.1073/pnas.1203707109.

Dwyer, J. G., J. R. Norris, and C. Ruckstuhl, 2010: Do climate models reproduce observed solar dimming and brightening over China and Japan? *J. Geophys. Res.*, **115**, D00K08, doi:10.1029/2009JD012945.

Gilgen, H., and A. Ohmura, 1999: The Global Energy Balance Archive. *Bull. Amer. Meteorol. Soc.*, **80**, 831–850.

Gilgen, H., M. Wild, and A. Ohmura, 1998: Means and trends of shortwave irradiance at the surface estimated from Global Energy Balance Archive Data. *J. Climate*, **11**, 2042–2061.

Koch, D., M. Schulz, S. Kinne and et al., 2009: Evaluation of black carbon estimations in global aerosol models. *Atmos. Chem. Phys.*, **9**, 9001–9026.

Norris, J. R., and M. Wild, 2007: Trends in aerosol radiative effects over Europe inferred from observed cloud cover, solar "dimming" and solar "brightening". *J. Geophys. Res.*, **112**, D08214, doi:10.1029/2006JD007794.

Ohmura, A., and H. Lang, 1989: Secular variation of global radiation over Europe, in Current Problems in Atmospheric Radition, edited by J. Lenoble and J. F. Geleyn, pp. 98-301, Deepak, Hampton, Va.

Ruckstuhl, C., and J. R. Norris, 2009: How do aerosol histories affect solar "dimming" and "brightening" over Europe?: IPCC-AR4 models versus observations. *J. Geophys. Res.*, **114**, D00D04, doi:10.1029/2008JD011066.

Shindell, D. T., J.-F. Lamarque, M. Schulz, and et al., 2012: Radiative forcing in the ACCMIP historical and future climate simulations. *Atmos. Chem. Phys. Discuss.*, **12**, 21,105–21,210, doi:10.5194/acpd–12– 21105–2012.

Taylor, K. E., R. J. Stouffer, and G. A. Meehl, 2012: An overview of CMIP5 and the experiment design. *Bull. Amer. Meteorol. Soc.*, **9**3, 485–498.

Wild, M., and E. Schmucki, 2011: Assessment of global dimming and brightening in IPCC- AR4/CMIP3 models and ERA40. *Climate Dyn.*, **37**, 1671–1688, doi:10.1007/s00382–010–0939–3.

Wild, M., 2009: Global dimming and brightening: A review. *J. Geophys. Res.*, **114**, D00D16, doi: 10.1029/2008JD011470.

Upcoming U.S. CLIVAR Events

also see our calendar online

To include an event in Variations or our online calendar, email **Jennifer Mays**.

U.S. CLIVAR Summit

July 9-11, 2013
Annapolis, MD
By invitation

AMS 15th Conference on Mesoscale Processes

August 6-9, 2013
Portland, OR

2013 Community Earth System Modeling Tutorial

August 12-16, 2013
NCAR, Boulder, CO

NOAA's 38th Climate Diagnostics and Prediction Workshop

abstract deadline July 15, 2013

October 21-25, 2013
College Park, MD

U.S. AMOC/U.K. RAPID International Science Meeting - AMOC Variability: Dynamics and Impacts

July 16-10, 2013
Baltimore, MD

NCAR ASP Research Workshop - Key Uncertainties in the Global Carbon-Cycle: Perspectives across terrestrial and ocean ecosystems

August 6-10, 2013
Boulder, CO

Analyses, Dynamics, and Modeling of Large Scale Meteorological Patterns Associated with Extreme Temperature and Precipitation Events

August 20-22, 2013
LBNL, Berkeley, CA

U.S. Climate Variability and Predictability Research Program (CLIVAR)
1717 Pennsylvania Ave NW, Suite 850
Washington, DC 20006
202.419.1801
www.usclivar.org
uscpo@usclivar.org
twitter.com/usclivar

U.S. CLIVAR acknowledges support from these U.S. agencies

This material was developed with federal support of NASA (AGS-093735), NOAA (NA06OAR4310119), NSF (AGS-0926904), and DOE (DE-SCOOO8494). Any opinions, findings, conclusions or recommendations expressed in this material are those of the authors and do not necessarily reflect the views of the sponsoring agencies.